Vacuum-ultraviolet $5d$-$4f$ luminescence of Gd^{3+} and Lu^{3+} ions in fluoride matrices

M. Kirm,[1] G. Stryganyuk,[2,3] S. Vielhauer,[1] G. Zimmerer,[2,3] V. N. Makhov,[1,4,*] B. Z. Malkin,[5] O. V. Solovyev,[5] R. Yu. Abdulsabirov,[5] and S. L. Korableva[5]

[1]*Institute of Physics, University of Tartu, Riia 142, Tartu 51014, Estonia*

[2]*Institut für Experimentalphysik, University of Hamburg, Luruper Chaussee 149, 22761 Hamburg, Germany*

[3]*Hamburger Synchrotronstrahlungslabor HASYLAB at Deutsches Elektronensynchrotron DESY, Notkestraße 85, 22607 Hamburg, Germany*

[4]*P.N. Lebedev Physical Institute, Leninskii Prospect 53, Moscow 119991, Russia*

[5]*Kazan State University, Kremlevskaya Street 18, 420008 Kazan, Russia*

(Received 22 November 2006; published 20 February 2007)

The VUV $4f^{n-1}5d$-$4f^n$ luminescence and luminescence excitation spectra of Gd^{3+} ($n=7$) in $LiGdF_4$, GdF_3, $LiYF_4:Gd^{3+}$, and $YF_3:Gd^{3+}$, and of Lu^{3+} ($n=14$) in $LiLuF_4$, LuF_3, and $LiYF_4:Lu^{3+}$ have been analyzed with high spectral resolution. In systems with intermediate electron-phonon coupling, zero-phonon lines, and phonon sidebands were observed. The excitation spectra of dilute systems exhibit rich fine structure originating from electronic origins of transitions and their phonon replica. Theoretical calculations explicitly taking into account a microscopic model of the crystal field and the crystal lattice vibrational spectra agree well with experimental data and are the basis for a safe analysis of the spectra.

DOI: 10.1103/PhysRevB.75.075111 PACS number(s): 78.55.Hx, 71.70.Ch, 63.20.Kr, 78.20.Bh

I. INTRODUCTION

Experiments on interconfigurational $4f^n$-$4f^{n-1}5d$ spectra of rare earth (RE) ions in large band gap matrices got started with the pioneering works of Feofilov[1] and Kaplyanskii and Feofilov[2] on the spectra of impurity divalent RE ions in alkaline-earth halides, as well as of Kaplyanskii *et al.*[3] on the spectra of trivalent cerium in alkaline-earth fluorides. In 1966, $4f^n \rightarrow 4f^{n-1}5d$ transitions of almost all trivalent RE ions (except Pm^{3+}, Gd^{3+}, and Lu^{3+}) in a CaF_2 matrix were reported by Loh.[4] Except from Ce^{3+} and Pr^{3+}, the transition energies are in the vacuum ultraviolet (VUV) spectral range where synchrotron radiation (SR) is the most powerful tool for spectroscopic researches.[5,6] VUV SR was applied for the first time to the studies of RE^{3+} $4f^n \rightarrow 4f^{n-1}5d$ excitations by Elias *et al.*[7] and Heaps *et al.*[8]

In the pioneering work of Yang and DeLuca,[9] it was found that Nd^{3+}, Er^{3+}, and Tm^{3+}, doped into fluorides, emit luminescence in the VUV spectral range, originating from $4f^{n-1}5d \rightarrow 4f^n$ radiative transitions (so-called $5d$-$4f$ luminescence). For the first half of the lanthanide series, transitions from the lowest $4f^{n-1}5d$ level into the $4f^n$ ground state are spin-allowed with short lifetimes (up to $\approx$50 ns). In the second half, such transitions are spin-forbidden (lifetimes in the μs range) because the spin of the lowest $4f^{n-1}5d$ state (so-called high-spin state) exceeds the spin of the ground $4f^n$ configuration. However, depending on the ion and the host, spin-allowed emission from the higher-lying low-spin $4f^{n-1}5d$ state (with the same value of spin as in the ground $4f^n$ state) can be also observed.[10,11]

Up to recently, RE^{3+} luminescence in VUV has been detected only from Nd^{3+}, Er^{3+}, and Tm^{3+}. However, our studies[12–14] have shown that VUV $5d \rightarrow 4f$ luminescence ($h\nu \sim 10$ eV) is also observed from Gd^{3+} and Lu^{3+} ions doped into some fluoride hosts with sufficiently wide energy band gaps. The observation of $5d$-$4f$ luminescence from the Gd^{3+} ion is rather unexpected because of the considerable number of closely spaced $4f^7$ levels in the same energy region as the $4f^6 5d$ states,[15] potentially enabling nonradiative relaxation from the lowest Gd^{3+} $4f^6 5d$ level to lower-lying $4f^7$ levels. However, at low temperatures a rather intense VUV luminescence has been detected from several materials containing Gd^{3+} ions. The situation is different for the Lu^{3+} ion, which has only a single $^1S_0$ level of the ground $4f^{14}$ electronic configuration. The reason why Lu^{3+} $5d$-$4f$ luminescence has never been detected earlier may arise from the fact that the corresponding photon energy is the highest among all RE^{3+} ions.

In the present paper, the results of a detailed investigation and characterization of VUV luminescence due to interconfigurational $5d$-$4f$ transitions in Gd^{3+} and Lu^{3+} ions in several fluorides are presented. In particular, results from stoichiometric Gd^{3+}- and Lu^{3+} fluorides (GdF_3, LuF_3, $LiGdF_4$, and $LiLuF_4$) are compared with results from Gd^{3+} and Lu^{3+} doped fluorides ($LiYF_4:Gd^{3+}$, $YF_3:Gd^{3+}$, $LiYF_4:Lu^{3+}$). Besides high-resolution luminescence spectra, allowing for an analysis of electron-phonon coupling, high-resolution excitation spectra have been measured as well. For comparison purposes, the Ce^{3+} ion with its simple electronic configuration in the $LiYF_4$ host has been included into our investigation. The phonon sidebands of the Ce^{3+} $5d$-$4f$ transitions yield great similarities with those of the Gd^{3+} ion, indicating that the details of the coupling of the $4f^{n-1}5d$ configuration to the matrix mainly depend on the matrix and only to a minor extent to the ion incorporated.

A comparison of experimental spectra with results of simulations performed for $LiYF_4$ doped with Ce^{3+} and Lu^{3+} ions will also be presented. The spectral envelopes were obtained in the framework of the exchange charge model of the ion-lattice interaction by making use of the spectral densities of correlation functions for the relative displacements of the impurity ion and its nearest ligands (eight fluorine ions),

which were calculated with the parameters of the real phonon spectrum of the crystal lattice.

II. EXPERIMENTAL DETAILS

The measurements were performed at the SUPERLUMI station of HASYLAB at DESY, using SR from the DORIS storage ring[16] for excitation. High-resolution VUV emission spectra were recorded with a 1-meter VUV monochromator and an open position-sensitive microchannel-plate (MCP) detector coated with CsI, at resolution intervals as small as 0.5 Å in second order.[17] The spectra were not corrected for the spectral response of the detection system. However, taking into account that the measured spectra cover usually a rather narrow spectral region and that the spectral sensitivity is smooth in the spectral range of interest, we believe that such correction will not result in any remarkable changes in the shape of the spectra. The excitation spectra of VUV emission and decay curves were recorded with a Pouey-type monochromator (typical spectral resolution interval $\Delta\lambda = 20$ Å) equipped with a CsI sensitized microsphere-plate detector. By applying deconvolution techniques, a time resolution of the detection system better than 0.1 ns was achieved. A 0.3 m Czerny-Turner monochromator-spectrograph SpectraPro-308i (Acton Research Inc.) with a R6358P (Hamamatsu) photomultiplier tube (PMT) was applied for measuring excitation spectra of UV/visible luminescence. Emission spectra in the UV/visible spectral range were recorded at the same spectrograph with a liquid nitrogen cooled CCD detector (Princeton Instruments Inc.). With a 300 grooves/mm grating, a spectral resolution of ~1 nm was achieved. These spectra were also not corrected for the spectral response of the detection system, i.e., relative intensity of lines observed in different spectral ranges can differ from that presented here.

During the present work, the VUV monochromator has been recalibrated by atomic lines. Compared to earlier experiments,[12,13] the absolute wavelength calibration was improved from ±0.2 Å to ±0.1 Å (corresponding to ±7 cm^{-1} at 82000 cm^{-1}). The relative accuracy of luminescence and excitation spectra is approximately the same because scattered light from the primary monochromator has been used for calibration of the secondary monochromators.

Single crystals of nominally pure $LiGdF_4$, $LiGdF_4$ doped with 0.05 at. % Ce^{3+}, $LiYF_4$ doped with 0.5 and 2.0 at. % Gd^{3+}, nominally pure $LiLuF_4$, $LiYF_4$ doped with 0.5, 1.0, and 5.0 at. % Lu^{3+}, $LiLuF_4$ and LuF_3, both doped with 0.1 at. % Ce^{3+}, were grown by the Czochralski and Bridgeman methods.[18,19] Powder samples of $LiYF_4$ doped with 1.0 and 10.0 at. % Gd^{3+}, and YF_3 doped with 1.0 at. % Gd^{3+}, were obtained by the high temperature diffusion technique. GdF_3 and LuF_3 powder samples were high-purity chemicals with a concentration of unintentional RE and other metals of 0.0005–0.001 %, and an oxygen concentration of 0.02–0.05 %. The crystalline samples were cleaved prior to mounting on the sample holder attached to a flow-type liquid helium cryostat. All measurements have been performed in an UHV environment.

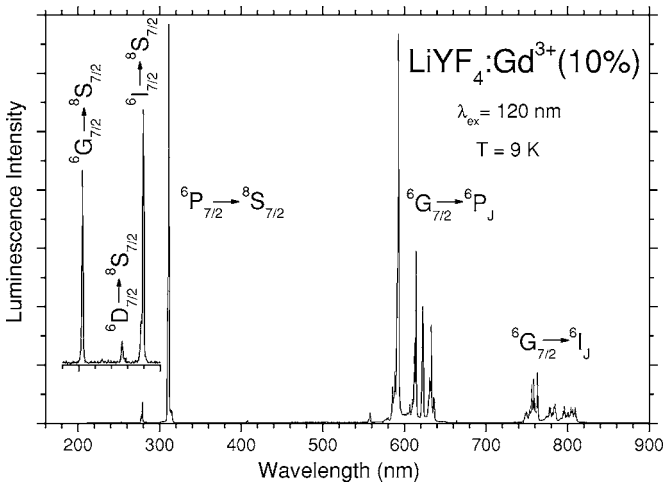

FIG. 1. Emission spectrum in the UV/visible/near IR range of the $LiYF_4:Gd^{3+}(10\%)$ powder sample excited by VUV (120 nm) radiation at 9 K, measured with the CCD detector. The spectrum in the inset was measured with the Pouey-type VUV monochromator. The intensities of both spectra are arbitrary. The assignments of emission lines to the corresponding Gd^{3+} $4f^7$-$4f^7$ transitions are given.

III. RESULTS AND DISCUSSION

A. $5d-4f$ transitions in Gd^{3+}

1. Experimental results on $LiGdF_4$, $LiYF_4:Gd^{3+}$, GdF_3, $YF_3:Gd^{3+}$

As it was mentioned above, Gd^{3+} $5d$-$4f$ luminescence was unexpected due to the fact that the $4f^7$ energy levels are very dense at high energies. Accordingly, it was supposed that radiative $5d$-$4f$ transitions in Gd^{3+} would be quenched due to energy transfer from d to f excitations and subsequent nonradiative relaxation into the lower f levels of Gd^{3+} from where emission takes place. Indeed, under VUV excitation, Gd^{3+} f-f lines in the UV, visible, and IR are observed in the emission spectra of Gd^{3+}-containing compounds (Fig. 1). In particular, the most intense line near 311 nm is due to transitions from the lowest excited $4f^7$ $^6P_{7/2}$ level to the Gd^{3+} $^8S_{7/2}$ ground state. The orange (590–640 nm) and IR (720–810 nm) luminescence, which are due to $4f^7$ $^6G_{7/2}$-^6P_J and $^6G_{7/2}$-^6I_J transitions in Gd^{3+},[20] are also observed under excitation to high energy levels of Gd^{3+}. However, at low temperature, VUV luminescence around 10 eV has been detected as well from several gadolinium fluoride crystals.[12–14] The energy level scheme and the main radiative and nonradiative transitions for the Gd^{3+} ion in some wide band gap (fluoride) hosts are shown in Fig. 2 (the energies of Gd^{3+} $4f^7$ levels were taken from Ref. 21).

The VUV emission spectrum from the $LiGdF_4$ crystal (Fig. 3) has a well-resolved fine structure which shows at least seven lines spread over ~500 cm^{-1}, extending into a wide sideband centered at ~78 900 cm^{-1}. The shortest-wavelength line at ~79 385 cm^{-1} has varying intensity for different excitation energies because of reabsorption which changes depending on the penetration depth of the exciting radiation. The spectra are similar for undoped and Ce^{3+}

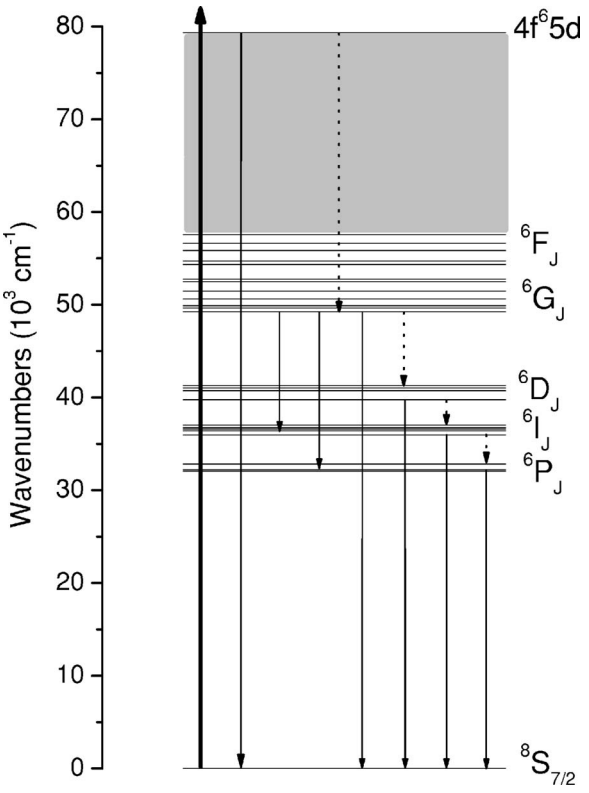

FIG. 2. Energy level pattern illustrating Gd^{3+} excitation by VUV radiation (bold solid arrow), relaxation (dotted arrows), and observed luminescence (thin solid arrows) in a wide band-gap fluoride matrix. The shaded area covers a range with many closely-spaced *f* levels, which cannot be distinguished in this scale.

doped samples. The VUV emission from crystalline $LiYF_4:Gd^{3+}(0.5\%)$ has nearly the same shape as that from the $LiGdF_4$ crystal but is slightly shifted to lower energies (by $\sim 110\ cm^{-1}$). The spectra from $LiYF_4:Gd^{3+}$ powder samples show only one pronounced line at $\sim 79\,220\ cm^{-1}$ and a wide sideband centered at $\sim 78\,900\ cm^{-1}$. The VUV emission spectra of GdF_3 and $YF_3:Gd^{3+}$ are situated at higher photon energies and show single structureless bands centered at $\sim 80\,000\ cm^{-1}$ and $\sim 79\,700\ cm^{-1}$, respectively. The decay times of VUV luminescence from all Gd^{3+}-containing samples are in the nanosecond range. At $T \sim 10$ K, the following decay times were measured: 2.8 ns for $LiGdF_4$, 2.5 ns for $LiYF_4:Gd^{3+}$, 0.97 ns for GdF_3, and 1.1 ns for $YF_3:Gd^{3+}$.

VUV luminescence from all Gd^{3+} compounds was observed only at low temperatures. As an example, in Fig. 4 the temperature dependence of the GdF_3 emission is shown. This dependence was approximated by the Mott formula, $I(T)/I(0)=[1+A\ \exp(-\varepsilon_a/k_BT)]^{-1}$ (shown in the inset of Fig. 4). An activation energy $\varepsilon_a \sim 400\ cm^{-1}$ for thermal quenching was obtained from the fit. Around 200 K, the VUV luminescence is quenched completely. For $LiYF_4:Gd^{3+}$, $\varepsilon_a \sim 530\ cm^{-1}$ and $620\ cm^{-1}$ for 10% and 1% doping concentrations were obtained. The values of ε_a are close to "characteristic" phonon energies of fluoride crystals, showing that the mechanism of thermal quenching can be treated as some kind of phonon-assisted nonradiative relaxation.

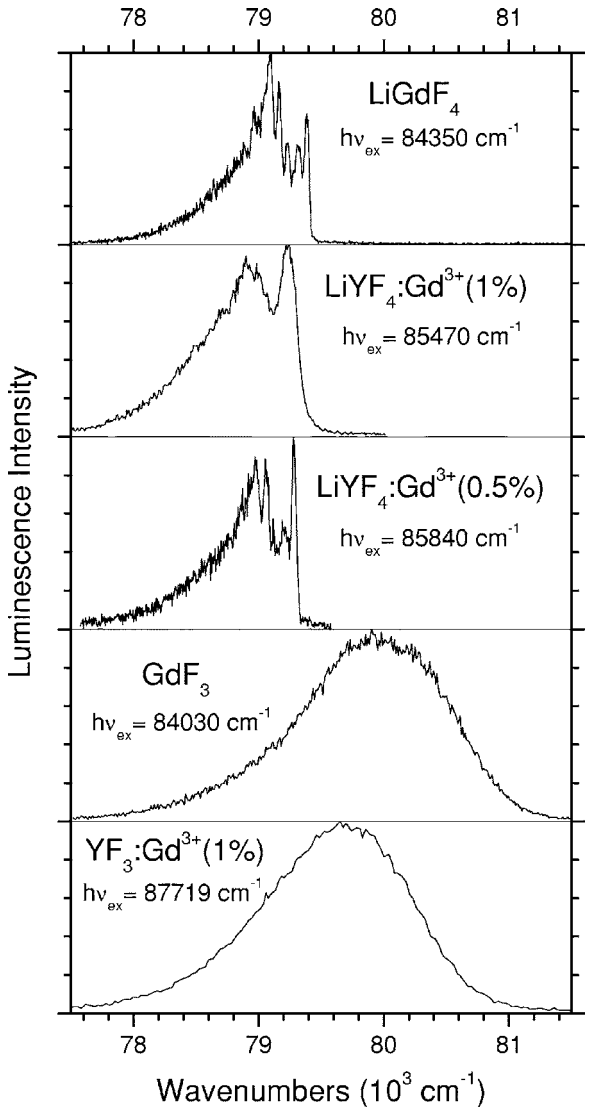

FIG. 3. High-resolution VUV emission spectra ($\Delta\lambda=0.8$ Å) of $LiGdF_4$ and $LiYF_4:Gd^{3+}(0.5\%)$ single crystals, and of $LiYF_4:Gd^{3+}(1\%)$, GdF_3 and $YF_3:Gd^{3+}(1\%)$ powder samples. The excitation energies are given in the figure. $T=10$ K.

The excitation spectrum of VUV emission from $LiGdF_4$ single crystal has a well-pronounced onset at $79\,000\ cm^{-1}$, overlapping with the shortest-wavelength line of the emission spectrum (Fig. 5). Hence, VUV luminescence is clearly correlated to the threshold of $Gd^{3+}\ 4f^7 \rightarrow 4f^6 5d$ excitation. Excitation spectra of UV/visible luminescence from $LiGdF_4$ have rather rich fine structure. Their onsets are slightly below the onset of the VUV emission (UV/visible luminescence is also observed under direct *f*-*f* excitation, however, the signal is too weak to be observed with SR.). Excitation spectra of different Gd^{3+} emissions from $LiYF_4:Gd^{3+}(10\%)$ (powder sample) have no pronounced fine structure but show a distinct threshold. Excitation spectra of all kinds of Gd^{3+} luminescence from $LiYF_4$ (both powder and crystalline samples) weakly (0.5, 1, 2 %) doped with Gd^{3+} have identical thresholds and the same shape at least in the range $79\,000-86\,000\ cm^{-1}$where the fine structure is clearly observed in all these spectra. The fine structure is most pro-

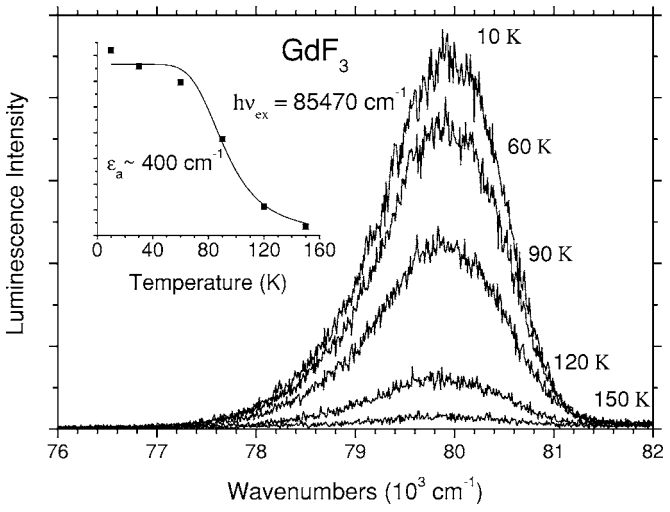

FIG. 4. Temperature dependence of the VUV luminescence from GdF_3. In the inset, the integrated intensity of the emission is plotted as a function of temperature, together with the simulation curve obtained as the best fit with the Mott formula.

nounced for the crystalline sample with the smallest (0.5%) concentration of Gd^{3+} (not shown).

The smooth-shaped excitation spectra of VUV emission from GdF_3 and $YF_3:Gd^{3+}$ have their thresholds near 83 000 cm^{-1} (Fig. 6). Similar to the case of $LiGdF_4$, excitation spectra of different kinds of luminescence from the stoichiometric compound GdF_3 have slightly different thresholds and shapes but all spectra lack fine structure. Excitation spectra of VUV and visible (595 nm) luminescence from $YF_3:Gd^{3+}$ coincide in the region near and right above the threshold, whereas the excitation spectrum of UV (311 nm) luminescence from this material shows slightly different shape (Fig. 6).

2. Assignment of VUV luminescence to 5d-4f radiative transitions in Gd^{3+}

The methodology proposed by Dorenbos[23] allows us to estimate the energy of the lowest $4f$-$5d$ transition in the RE^{3+} ion doped into a particular host if the value of this energy is known for any other RE^{3+} ion, e.g., for Ce^{3+}, which has been extensively studied in many matrices. According to Ref. 23, the energy for the lowest spin-allowed $4f$-$5d$ transition in a RE^{3+} ion is given by

$$E^{\mathrm{RE},s-a} = 49340\ \mathrm{cm}^{-1} - D(A) + \Delta E^{\mathrm{RE,Ce}} \qquad (1)$$

where 49 340 cm^{-1} is the energy of the lowest $4f$-$5d$ transition in the free Ce^{3+} ion, $D(A)$ is the crystal field depression energy for the compound A, and $\Delta E^{\mathrm{RE,Ce}}$ is the energy difference between the first spin-allowed $4f$-$5d$ transition in the RE^{3+} and Ce^{3+} ions. The basis of this approximation is the fact that the crystal field depression is not sensitive to the individual ion, $D(A)$ being an average of the $D(\mathrm{RE}^{3+},A)$ values for different RE^{3+} ions. In this approximation, the quantity $\Delta E^{\mathrm{RE,Ce}}$ is independent from the host and can be regarded as an intrinsic property of the respective ion, being equal to 45 800 cm^{-1} for $\Delta E^{\mathrm{Gd,Ce}}$.[23] Using the energy difference between the maxima of broad Gaussian-like bands (corresponding to strong electron-phonon coupling), the methodology can be applied only to GdF_3 and $YF_3:Gd^{3+}$. It can be extended, however, to the estimation of the energies of zero-phonon lines (ZPLs) because the Stokes shift $\Delta S(A)$ between absorption and emission bands is characteristic for the host A but nearly independent from the RE^{3+} ion.[23] For $LiGdF_4$ and $LiYF_4:Gd^{3+}$, the energies of the lowest $4f$-$5d$ ZPLs are therefore estimated according to

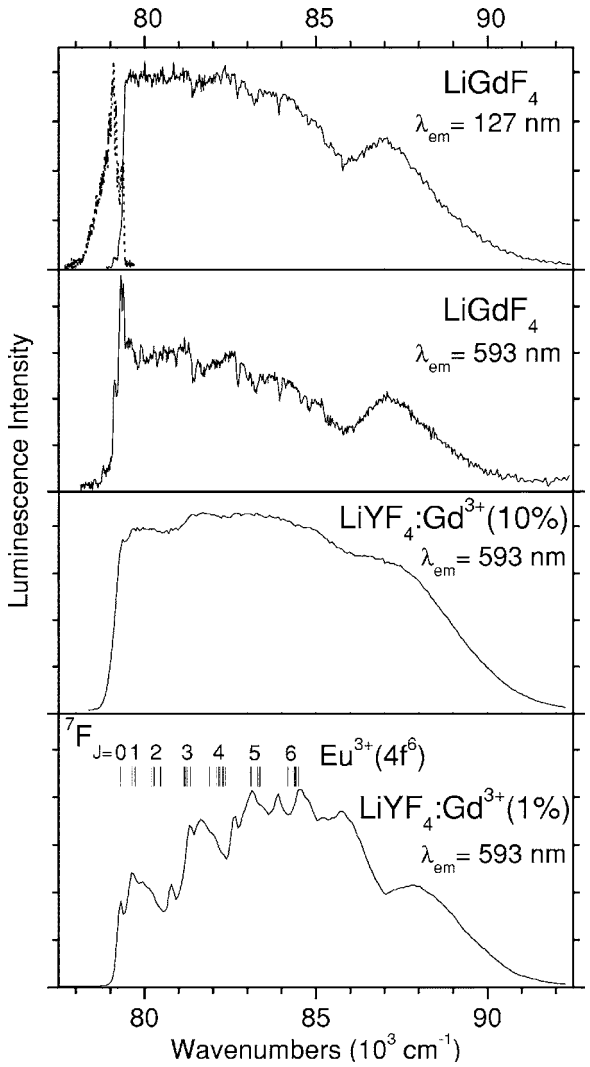

FIG. 5. High-resolution excitation spectrum ($\Delta\lambda = 0.8$ Å) of the Gd^{3+} $5d$-$4f$ emission from $LiGdF_4$ (crystal), measured at 127 nm (78 740 cm^{-1}), together with the respective high-resolution emission spectrum excited by 119 nm (84 033 cm^{-1}) photons (upper part of the figure). All other curves are high-resolution excitation spectra of the Gd^{3+} $^6G_{7/2}$-$^6P_{7/2}$ emission at 593 nm from $LiGdF_4$ (crystal), from $LiYF_4:Gd^{3+}(10\%)$ and $LiYF_4:Gd^{3+}(1\%)$ (powder samples). $T = 10$ K. The energy levels of the Eu^{3+} $^7F_{J=0,6}$ multiplet in $LiYF_4$ (Ref. 22) are added for comparison (see text for details).

$$E_{ZPL}^{Gd} = E_{ZPL}^{Ce} + \Delta E^{Gd,Ce}. \qquad (2)$$

From the excitation spectrum of $LiGdF_4$ doped with 0.05% Ce^{3+}, the ZPL energy of the lowest Ce^{3+} $4f$-$5d$ transition in $LiGdF_4$ (Fig. 7) was determined (33 615 cm^{-1}). The

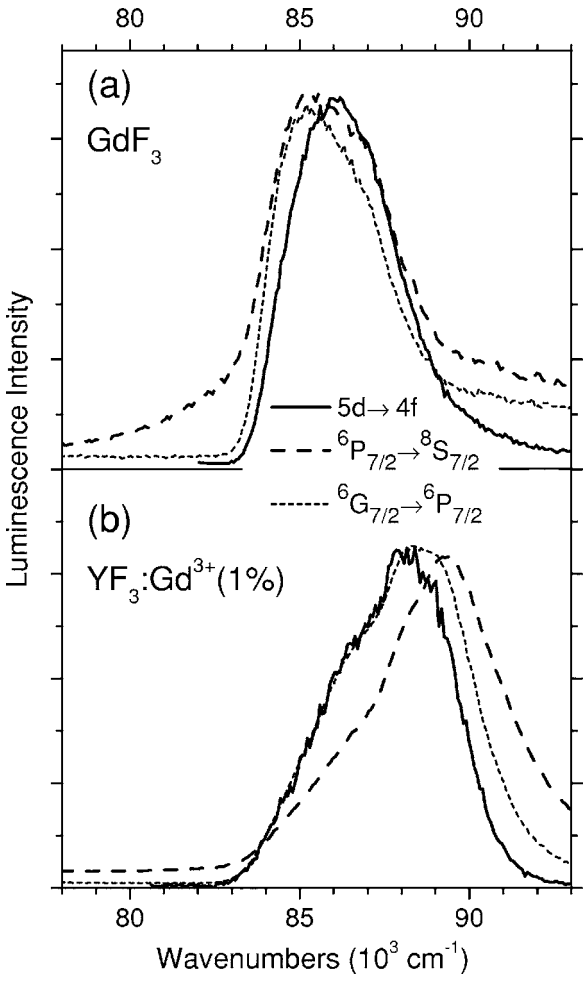

FIG. 6. Excitation spectra ($\Delta\lambda = 3$ Å) of Gd^{3+} 5*d*-4*f*, $^6P_{7/2}$-$^6S_{7/2}$ and $^6G_{7/2}$-$^6P_{7/2}$ emissions from GdF_3 and $YF_3:Gd^{3+}(1\%)$ powder samples. $T = 10$ K.

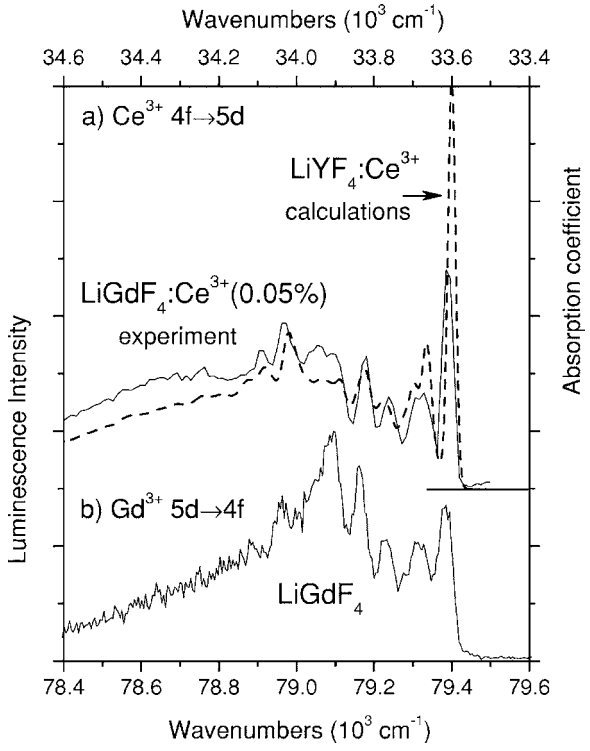

FIG. 7. (a) High-resolution excitation spectrum of $LiGdF_4:Ce^{3+}(0.05\%)$ monitoring Gd^{3+} $^6P_{7/2} \rightarrow {}^8S_{7/2}$ 311 nm emission and calculated Ce^{3+} 4*f*-5*d* absorption spectrum of $LiYF_4:Ce^{3+}(0.05\%)$ (upper wave number scale). (b) High-resolution VUV emission spectrum ($\Delta\lambda = 0.8$ Å) of $LiGdF_4$ (lower wave number scale). $T = 10$ K.

estimated energy of the ZPL of the lowest Gd^{3+} $4f^7$-$4f^6 5d$ transition then is 79 415 cm^{-1}, which is close to the threshold of the excitation spectrum of $LiGdF_4$ VUV emission as well as to the energy of the shortest-wavelength emission line from this crystal (79 385 cm^{-1}). Similar estimates for $LiYF_4:Gd^{3+}$ yield 79 250 cm^{-1} for the ZPL of the lowest Gd^{3+} $4f^7$-$4f^6 5d$ transition, taking 33 450 cm^{-1} for the ZPL of the lowest 4*f*-5*d* transition of Ce^{3+} in $LiYF_4:Ce^{3+}$.[24] The estimate agrees well with experiment (79 278 cm^{-1}).

For GdF_3 and $YF_3:Gd^{3+}$, Eq. (1) can be applied directly. The depression energies of GdF_3 and YF_3 are 10 878 cm^{-1} and 9915 cm^{-1}, respectively.[23] From Eq. (1), the lowest Gd^{3+} 4*f*-5*d* transition energies are 84 262 cm^{-1} (GdF_3) and 85 225 cm^{-1} ($YF_3:Gd^{3+}$). Since the first broad maxima in the excitation spectra of Gd^{3+} 4*f*-5*d* emission in GdF_3 and $YF_3:Gd^{3+}$ result from an overlap of transitions to various sublevels of the first crystal field 5*d* component, a comparison with the estimates will be misleading. However, the estimates may be better compared with the maxima in the VUV emission spectra, taking into account the Stokes shifts ΔS for these compounds given in Ref. 23, 5567 cm^{-1} for GdF_3 and 5444 cm^{-1} for YF_3. The estimated maxima of Gd^{3+} 5*d*-4*f* emission in GdF_3 and $YF_3:Gd^{3+}$ are 78 695 and 79 781 cm^{-1}. For $YF_3:Gd^{3+}$ the estimate agrees well with the experimental value (79 700 cm^{-1}). For GdF_3, the experimental value (80 000 cm^{-1}) exceeds the estimate considerably. Note, however, the energy parameters for Gd^{3+} 4*f*-5*d* transitions in GdF_3 given in Ref. 23 were obtained using data from a single paper and may therefore be less accurate than the parameters of $YF_3:Gd^{3+}$, resulting in less reliable estimates.

Referring to the good agreement between theoretical estimates and experimental transition energies, the VUV luminescence observed is ascribed to Gd^{3+} transitions from the lowest $4f^6$ 5*d* level to the $4f^7$ $^8S_{7/2}$ ground state. The assignment is supported by the following arguments. The VUV luminescence is observed in stoichiometric *and* weakly doped compounds, excluding an excitonic nature, which would be an alternative explanation. The decay time of a few nanoseconds is expected for the $4f^6$ 5*d*-$4f^7$ radiative transitions in Gd^{3+}, which are spin-allowed because the lowest Gd^{3+} $4f^6 5d$ level has the same spin as the ground state. Only one fast transition originating from the lowest $4f^6$ 5*d* level to the ground state is observed because of the absence of spin-orbit splitting for the ^8S ground term of Gd^{3+}. Transitions from the lowest $4f^6 5d$ level to excited $4f^7$levels are spin- and parity forbidden, i.e., the corresponding luminescence should be extremely weak. The crystal-field splitting of Gd^{3+} 5*d* level in GdF_3 is expected to be smaller than in $LiGdF_4$ because of the higher coordination number for Gd^{3+}

(9 instead of 8), and accordingly the Gd^{3+} $4f^6 5d$-$4f^7$ luminescence is observed at higher energy in GdF_3.

3. Specific nature of the 5d-4f luminescence from Gd^{3+}: spin selection rules for nonradiative transitions, phonon fine structure

The dense $4f^7$ level system overlapping with the lowest Gd^{3+} $4f^6 5d$ level might open an efficient nonradiative relaxation channel, quenching the radiative decay. However, the rather strong emission intensities and the lifetimes in the ns range clearly show that the branching between radiative and nonradiative transitions favors the radiative decay at low temperatures. A selection rule must therefore suppress the nonradiative channel. The spin multiplicity of the lowest $4f^6 5d$ level of Gd^{3+} is eight, whereas the $4f^7$ levels of Gd^{3+} closest to the $4f^6 5d$ level are spin doublets or quartets.[25] As a consequence, the nonradiative channel is heavily spin-forbidden.

The crystal-field splitting of the Gd^{3+} ground state is extremely small,[26] i.e.—within the spectral resolution interval—only one ZPL is expected in the Gd^{3+} VUV emission, corresponding to the electronic origin of the $4f^6 5d$-$4f^7$ $^8S_{7/2}$ transition. The $5d$-$4f$ luminescence spectra, however, yield several narrow lines, the origin of which is discussed below. For this purpose, the $5d$-$4f$ emission spectrum of $LiGdF_4$ is compared with the excitation spectrum for $LiGdF_4$:Ce(0.05%) at the edge of the Ce^{3+} f-d excitation (Fig. 7). A striking similarity is observed. This is also the case for $LiYF_4$:Gd^{3+}. For the Ce^{3+} ion with only one $4f$ electron, a single ZPL is expected for $4f$-$5d$ absorption (excitation) to each crystal-field $5d$ component. All other structures arise from electron-phonon transitions (note the low doping level). The one-to-one correspondence between the Ce^{3+} excitation spectrum and the Gd^{3+} $5d$-$4f$ emission proves that the fine structure in Gd^{3+} $5d$-$4f$ emission is due to one ZPL and its phonon replica. The shape of the spectrum with a ZPL, a few narrow vibronic lines, and a wide lower-energy vibronic side band is typical for intermediate electron-phonon coupling. This is confirmed by an estimate of the Huang-Rhys parameter $S \sim 1$ from the energy difference between the ZPL and the maximum of the wide side band, taking into account the phonon spectrum of $LiGdF_4$.[27] An excellent agreement was obtained also between experimental spectra and calculations of the absorption spectrum for $LiYF_4$:Ce^{3+} (see Fig. 7). This will be discussed in Sec. III C.

The Stokes shift of $\sim 6000\ cm^{-1}$ observed in GdF_3 and YF_3:Gd^{3+} for Gd^{3+} $4f^7$-$4f^6 5d$ transitions is more than 10 times larger than the maximum phonon energy in RE trifluorides,[28] i.e., the Huang-Rhys parameter S exceeds 5 in these matrices, corresponding to strong electron-lattice coupling. This explains the absence of any vibronic fine structure in the emission and excitation spectra.

4. Excitation spectra of Gd^{3+} 5d-4f luminescence and comparison with the energy level pattern of Eu^{3+}

In this section, the excitation spectra presented in Fig. 5 will be discussed. They have a pronounced threshold originating from the onset of $4f$-$5d$ excitations (see Secs. III A 1 and III A 2). They all agree concerning the decrease at high energies. This decrease is due to the onset of host absorption. In between, however, two types of spectra are observed. One type yields a level of emission, which is nearly independent from the excitation energy. This is true for optically dense systems [either $LiGdF_4$ or $LiYF_4$:Gd^{3+}(10%)], *and* an emission with a *fast* decay. The other type yields fine structure in an optically dense system ($LiGdF_4$) and a *slow* emission (593 nm) but also in an optically thin system [$LiYF_4$:Gd^{3+}(1%)] with fast emission.

The first type corresponds to total absorption of the exciting radiation with subsequent relaxation into the emitting level. Provided the quantum efficiency is independent from the penetration depth of the exciting radiation, in this case no distinct fine structure can show up. It is well known, however, that energy transport towards the surface and surface quenching results in a modulation of excitation spectra with a correlation between minima in penetration depths (maxima in absorption) and minima in the excitation spectrum.[29] In the optically dense system $LiGdF_4$, both is observed: on a ns time scale, energy transport to the surface is obviously inefficient ($5d$-$4f$ emission). On a time scale corresponding to the long lifetime of the 593 nm emission, energy transport to the surface and surface quenching modulates the excitation spectrum. The minima in the excitation spectrum are therefore ascribed to maxima of the absorption coefficient, whatever the nature of these maxima may be. The $5d$-$4f$ excitation spectrum in the optically thin system $LiYF_4$:Gd^{3+}(1%) supports this statement. On a ns time scale, in the doped system the energy transport to the surface is even less efficient than in the optically dense system $LiGdF_4$. Therefore, the maxima observed are maxima in absorption. They are clearly correlated to the minima in the excitation spectrum of the 593 nm emission [apart from the small matrix shift of $170\ cm^{-1}$ (Sec. III A 1)]. More details will be given in a forthcoming paper.[30]

The absorption maxima may be of electronic origin, they could originate from vibronic sidebands, or there may be a superposition of both. The splitting between distinct maxima is of the order of $1000\ cm^{-1}$, by far exceeding the splitting of vibronic sidebands as has been observed in the emission spectra (Sec. III A 3). Therefore, electronic excitations have to be considered. It is certainly too simple to discuss them in terms of the f^7 configuration which does not interact with the $5d$ level. On the contrary, the levels of the $4f^6 5d$ configuration have to be taken into account.

To the best of our knowledge, no calculations of $4f^7$-$4f^6 5d$ transitions in Gd^{3+} were published in the literature. However, rather extensive studies have been performed for $4f^7$-$4f^6 5d$ transitions in Eu^{2+},[31,32] which is isoelectronic to the Gd^{3+} ion. The structure observed for $4f^7$-$4f^6 5d$ transitions in Eu^{2+} was traced back to the energy level pattern of the $4f^6$ core in the $4f^6 5d$ state. The levels of the $4f^6$ core were approximated by the well-known $4f^6$ level scheme of Eu^{3+}. Rather good agreement between the measured peaks and the Eu^{3+} $4f^6$ levels was obtained.[31]

In analogy to the procedure of Ryan *et al.*,[31] we included in Fig. 5 the Eu^{3+} $4f^6$ levels of $LiYF_4$:Eu^{3+} taken from Ref.

22 for comparison with the fine structure observed above threshold of Gd^{3+} $4f^7$-$4f^6 5d$ excitation. The Eu^{3+} levels were arranged in a way that the Eu^{3+} $4f^6$ ground state coincides with the Gd^{3+} $4f^7$-$4f^6 5d$ ZPL. The energy range of the lower ^7F_J multiplets of the Eu^{3+} $4f^6$ configuration matches well the energy spread for the Gd^{3+} electronic transitions under discussion. Therefore, the fine structure is ascribed to electronic levels of the $4f^6 5d$ configuration. A one-to-one correspondence between the maxima and the Eu^{3+} levels, however, cannot be expected in view of the rudeness of the model.

B. 5*d*-4*f* transitions in Lu^{3+}

1. Experimental results on $LiLuF_4$, $LiYF_4:Lu^{3+}$, and on LuF_3 at low temperatures

VUV emission from the $LiLuF_4$ crystal consists of a line at 80 910 cm^{-1} and a wide sideband centered at ~80 180 cm^{-1}, whereas the luminescence spectrum from the $LiYF_4:Lu^{3+}(0.5\%)$ crystal has a steep high-energy onset at ~81 100 cm^{-1} followed by distinct lines and a sideband centered at ~80 630 cm^{-1}, i.e. the emission spectrum from $LiYF_4:Lu^{3+}$ is narrower than the one from $LiLuF_4$ (Fig. 8). The VUV emission from the $LuF_3:Ce^{3+}$ single crystal and from the undoped powder sample of LuF_3 consists of a single broad band centered at ~80 500 cm^{-1} (Fig. 9). VUV luminescence from all studied lutetium compounds has a long lifetime beyond the experimental limit (longer than ~1 μs) and is thermally quenched near 200 K. The VUV luminescence is ascribed to Lu^{3+} 5*d*-4*f* transitions. The long lifetime indicates a spin-forbidden character of 5*d*-4*f* transition. The assignment will be confirmed in Sec. III B 2.

The excitation spectrum of VUV emission from the $LiLuF_4$ crystal has a smooth rise above 81 000 cm^{-1} with some faint structures, and two pronounced peaks at 81 760 and 83 150 cm^{-1} (Fig. 8). In the case of $LiYF_4:Lu(5\%)$, a steep threshold at 81 760 and two lines just above threshold at 81 950 cm^{-1} and 82 240 cm^{-1} are observed. An additional pronounced rise shows up at 83 170 cm^{-1}. At the low-energy side of the 81 760 cm^{-1} threshold, weak features are observed in an enlarged scale, corresponding to the faint structures of the rising part of the $LiLuF_4$ spectrum. The excitation spectrum of the LuF_3 5*d*-4*f* luminescence has a threshold near 82 700 cm^{-1} and does not show any fine structure (Fig. 9).

2. Assignment of VUV luminescence to 5d-4f radiative transitions in Lu^{3+}

The energies for the lowest Lu^{3+} 4*f*-5*d* transitions in $LiLuF_4$ and in the $LiYF_4$ matrix are estimated according to[23]

$$E_{ZPL}^{Lu,s-a} = E_{ZPL}^{Ce} + \Delta E^{Lu,Ce}. \quad (3)$$

$\Delta E^{Lu,Ce}$=49 170 cm^{-1} given in Ref. 23 may be rather uncertain because it is solely based on one paper on gaseous Lu^{3+}. The energies of the ZPLs for Ce^{3+} 4*f*-5*d* transitions (33 130 cm^{-1} in $LiLuF_4:Ce^{3+}$ and 33 450 cm^{-1} in $LiYF_4:Ce^{3+}$) are taken from Ref. 24. Equation (3) then yields the values of the spin allowed Lu^{3+} $4f^{14}$-$4f^{13}5d$ ZPLs

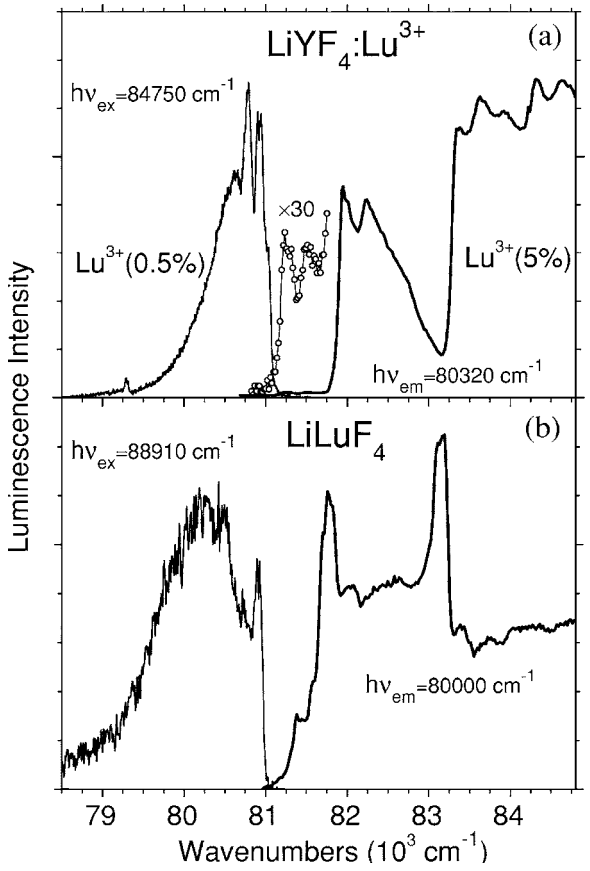

FIG. 8. High-resolution VUV emission spectra ($\Delta\lambda$=0.8 Å) from $LiYF_4:Lu^{3+}(0.5\%)$ (a) and $LiLuF_4$ (b) single crystals, together with the respective high-resolution excitation spectra. In the case of $LiYF_4:Lu^{3+}$, a sample with 5% concentration of Lu^{3+} ions was chosen for excitation spectrum measurement in order to get a stronger signal in the range from 81 000 cm^{-1} to 81 750 cm^{-1}. This part of the excitation spectrum is shown also in enlarged (×30) scale. T=11.5–12 K.

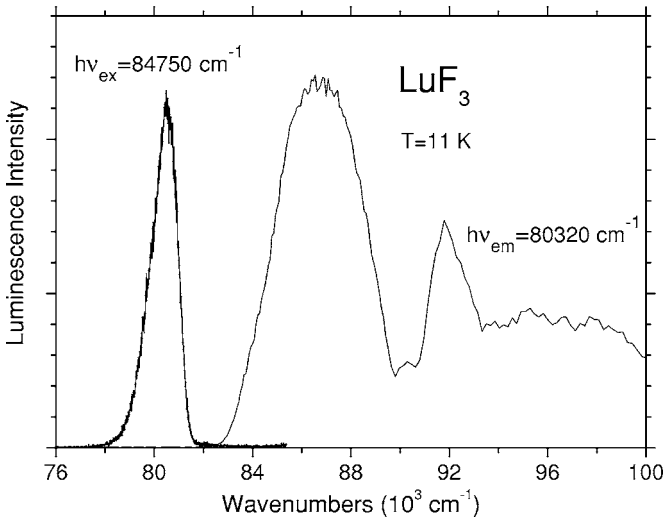

FIG. 9. High-resolution VUV emission spectrum and excitation spectrum of VUV emission from LuF_3 powder sample. T=11 K.

in $LiLuF_4$ and $LiYF_4:Lu^{3+}$: 82 300 and 82 620 cm^{-1}. These values are considerably larger than the energies of the pronounced maxima in the excitation spectra below 82 000 cm^{-1}.In view of the uncertainly of $\Delta E^{Lu,Ce}$, it is not possible to take the estimates as the basis for an assignment of any structure to a ZPL. However, the estimates clearly prove that the strong signals in the excitation spectra around 82 000 cm^{-1} arise from spin-allowed transitions in Lu^{3+} from the $4f^{14}{}^1S_0$ state to the lowest low-spin ($S=0$) state of the excited $4f^{13}5d$ configuration.

The calculations following the methodology of Dorenbos can be extended to the spin-forbidden $4f$-$5d$ transitions since the energy difference, $\Delta E_{RE}^{sa,sf}$, between the spin-allowed and the spin-forbidden $4f$-$5d$ excitation energy is merely a property of the respective ion but is nearly independent on the host

$$E_{ZPL}^{Lu,s\text{-}f} = E_{ZPL}^{Ce} + \Delta E^{Lu,Ce} - \Delta E_{Lu}^{sa,sf}. \quad (4)$$

Unfortunately, the value of $\Delta E_{Lu}^{sa,sf}$ is not known. However, taking into account the decreasing trend of the energy splitting between spin-allowed and spin-forbidden $4f$-$5d$ transitions from Tb^{3+} to Yb^{3+}, and that in Yb^{3+} this splitting is of the order 1500 cm^{-1},[33] we have reasons to argue that $\Delta E_{Lu}^{sa,sf} \leq 1500$ cm^{-1}. The estimates of ZPL energies for spin-forbidden Lu^{3+} $4f$-$5d$ transitions in $LiLuF_4$ and $LiYF_4$ hosts are $>80\,800$ cm^{-1} and $>81\,120$ cm^{-1}, respectively. The lower limits of these estimates are close to the weak features observed in the excitation spectra of $LiLuF_4$ and $LiYF_4:Lu^{3+}$ and to the high-energy tails of the respective luminescence curves. The VUV emission is therefore ascribed to spin-forbidden transitions from the lowest high-spin ($S=1$) level of the $4f^{13}5d$ configuration to the Lu^{3+} $4f^{14}{}^1S_0$ ground state.

In contrast to $LiGdF_4$ and $LiYF_4:Gd^{3+}$ where strong ZPLs at the short wavelength edges of spectra are clearly observed, the $5d$-$4f$ spectra from $LiLuF_4$ and $LiYF_4:Lu^{3+}$ do not show ZPLs (within the experimental sensitivity). The short-wavelength tail of the Lu^{3+} $5d$-$4f$ emission overlaps with the long wavelength tail of the weak structure in the excitation spectrum. Obviously, the transition probability for the pure electronic spin-forbidden transition is extremely small, so that only phonon-assisted transitions show up in the spectra. The sharp lines observed in Lu^{3+} $5d$-$4f$ luminescence in $LiLuF_3$ and $LiYF_4:Lu^{3+}$ are therefore ascribed to phonon-assisted transitions, merging into a sideband. The electronic origin may be estimated from the crossing of the emission and excitation spectra ($\sim$81 000 cm^{-1}). The absence of the ZPL will be further discussed in Sec. III C.

Concerning LuF_3, the VUV emission is ascribed as well to the spin-forbidden Lu^{3+} $5d$-$4f$ transitions. Whereas the shape of the emission band corresponds to the strong coupling case, the first excitation band observed in the excitation spectrum is not the counterpart of emission but is mainly due to a convolution of spin-allowed excitations into different crystal field components. Therefore, e.g., the energetic difference between the maxima in emission (80 500 cm^{-1}) and excitation (87 000 cm^{-1}) does not correspond to the Stokes shift. One may speculate that the asymmetric shape of the excitation spectrum around 84 000 cm^{-1} arises from the spin-forbidden excitation band, indicating a rough estimate of the Stokes shift 4000 cm^{-1} and an electronic origin at 82 000 cm^{-1}.

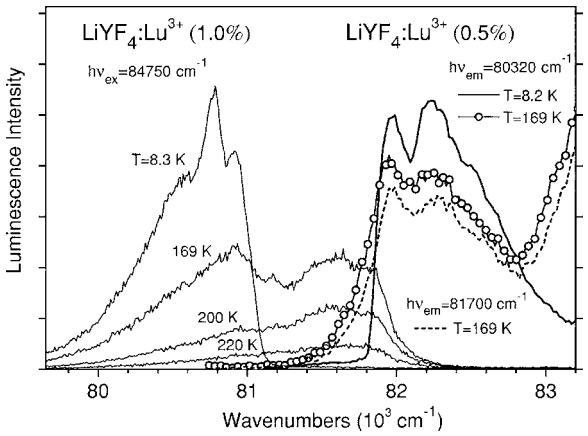

FIG. 10. Temperature dependence of the Lu^{3+} VUV emission ($\Delta\lambda \sim 2$ Å) from $LiYF_4:Lu^{3+}$(1%) single crystal in the temperature range from 8.3 to 220 K, excited by 118 nm (84 750 cm^{-1}) photons; high-resolution excitation spectra of the low- and high-energy VUV emissions from $LiYF_4:Lu^{3+}$(0.5%) crystal at temperatures 8.2 and 169 K.

Although no ZPLs are observed, the fine structure of the luminescence spectra of $LiLuF_4$ and $LiYF_4:Lu^{3+}$ indicates intermediate coupling. Taking into account the estimate of the electronic origin, the effective phonon frequencies (400 cm^{-1}) (Ref. 27) of the respective lattice and the energetic position of the smooth luminescence sidebands, $S \sim 2$ is obtained. The Stokes shift between absorption and emission for $4f^{13}5d$-$4f^{14}$ transitions in LuF_3 ($\sim$4000 cm^{-1}) is considerably larger than in $LiYF_4$ and $LiLuF_4$, i.e., Huang-Rhys parameter $S>5$ in LuF_3, which is in agreement with strong coupling (absence of any vibronic fine structure).

3. *Temperature dependence of* Lu^{3+} $5d$-$4f$ *luminescence*

As already mentioned, Lu^{3+} $5d$-$4f$ luminescence in the materials studied is thermally quenched at temperatures $T>200$ K. However, as a function of temperature, an additional higher-energy emission band appears at temperatures $T>100$ K. This band is observed from all studied Lu^{3+}-containing compounds independent of the Lu^{3+} concentration, i.e., this is the property of the Lu^{3+} ion but not of the matrix. The results for $LiYF_4:Lu^{3+}$ are shown in Fig. 10. Compared to Fig. 8, the vibronic structures are broader. This is not only due to the larger resolution interval used (2 Å) but also to thermal broadening. The excitation spectrum measured at 8.2 K broadens as well at elevated temperatures. At intermediate temperatures where both bands coexist, the excitation spectra of both bands coincide.

As was discussed above, the transition probability for spin-forbidden $5d$-$4f$ radiative transitions from the lowest high-spin ($S=1$) $4f^{13}5d$ state of Lu^{3+} is very small. However, with increasing temperature, an additional decay channel for the lowest $4f^{13}5d$ level is opened, namely thermal population of the higher-lying low spin ($S=0$) $4f^{13}5d$ state,

from which the $5d$-$4f$ raditive transition is spin-allowed. The additional emission band observed is ascribed to the spin-allowed $5d$-$4f$ luminescence.

Under thermal equilibrium population of both levels, the intensity ratio for the emission from these levels is determined by the ratio of products of the level population and transition probability from the level. Since the energy separation between high- and low-spin $4f\,^{13}5d$ states in Lu^{3+} is small (as a rough approximation, either the energy separation of the envelopes of both bands or the estimates of electronic origins in Sec. III B 2 may be taken), the emission from the low-spin $4f\,^{13}5d$ state can become intense at rather low temperatures. At $T\sim 150$ K ($LiYF_4:Lu^{3+}$), the intensities of both bands are approximately the same. For the level separation of 823 cm^{-1} obtained from calculations (see Sec. III C below), the ratio of transition probabilities for spin-allowed and spin-forbidden $5d$-$4f$ transitions is estimated as being $\sim 3\times 10^3$, which is reasonable. It should be noted that due to the specific mechanism of population of this low-spin $4f^{13}5d$ state, the decay kinetics for the high-energy band is controlled by lifetime for spin-forbidden transition and accordingly is slow. A similar effect was observed for Er^{3+} spin-allowed and spin-forbidden $5d$-$4f$ luminescence from the $LiYF_4:Er^{3+}$ crystal[34] but at much higher temperatures $\sim$800 K, since the splitting between high- and low-spin $5d$ states of the Er^{3+} ion is $\sim$3300 cm^{-1}.[33]

4. Excitation spectra of Lu^{3+} *5d-4f luminescence*

In this section, only a few aspects of the excitation spectra (Fig. 8) will be discussed. The excitation spectrum of Lu^{3+} $5d$-$4f$ emission in $LiYF_4:Lu^{3+}(5\%)$ yields pronounced maxima which are ascribed to crystal-field components and phonon sidebands of the $4f\,^{13}5d$ configuration. More details are given in Sec. III C where the spectrum will be compared with calculations.

The most striking features of the $LiLuF_4$ spectrum are the maxima at 81 760 cm^{-1} and 83 150 cm^{-1}. In an earlier publication, they were ascribed to ZPLs of spin-forbidden and spin-allowed Lu^{3+} $4f\,^{14}$-$4f\,^{13}5d$ transitions.[24] In view of the new results of the present paper, this interpretation is no longer valid. The pronounced peaks correspond well to the thresholds observed in the excitation spectrum of the dilute system $LiYF_4:Lu^{3+}(5\%)$ (Fig. 8). Hence, they correspond to excitation with large penetration depths where all kind of surface quenching is of minor importance. Indeed, the general behavior of the $LiLuF_4$ spectrum can be modeled, taking into account diffusive-type energy transfer from the bulk to the surface and surface quenching. The strong peaks arise from excitations in the bulk, which are not affected by surface quenching. More details are given elsewhere.[30]

C. Electron-phonon interaction in the $4f^n$-$4f^{n-1}5d$ electronic configurations of RE^{3+} ions and simulations of the $4f^n$-$4f^{n-1}5d$ spectra

1. General theory of electron-vibrational $4f^n$-$4f^{n-1}5d$ *spectra in the adiabatic approximation*

To simulate interconfigurational $4f$-$5d$ spectral envelopes, we use the approach derived in Ref. 35 and generalized for the spin-forbidden transitions. This approach involves calculations of crystal field parameters for a $5d$ electron as explicit functions of lattice ion's coordinates in the framework of the exchange charge model,[36] numerical diagonalization of the effective impurity ion Hamiltonian containing energies of electrostatic Coulomb and exchange interactions between electrons, spin-orbit interactions and the crystal field interactions for the ground ($4f^n$) and excited ($4f^{n-1}5d$) electronic configurations; calculations of the $5d$-electron-phonon coupling constants, and simulations of the band shapes by making use of the realistic phonon spectrum of the host crystal lattice. The crystal field model was improved, in comparison with Ref. 35, by taking into account the extended charge distributions of a $5d$ electron and ligands' outer electrons in calculations of the electrostatic component of the ligand field.[37] An energy gap Δ between the excited and ground configurations is treated as a fitting parameter. The Hamiltonian of the $5d$-electron-phonon interaction, linear in dynamic displacements $\boldsymbol{u}(Ls)$ of the lattice ions

$$H_{el\text{-}ph}=\sum_{L,s,\alpha} V_\alpha(Ls)[u_\alpha(Ls)-u_\alpha(00)] \tag{5}$$

[here unit cells and ions in the cell are labeled by L and s, respectively, with the impurity ion having the (00) label] is considered within the cluster approximation: modulation of the crystal field by ligand vibrations is considered only. The electronic operators $V_\alpha(Ls)$ are defined by the coupling constants, which can be obtained by direct differentiation of corresponding crystal field parameters with respect to the lattice ion coordinates. Lattice vibrations are considered in the harmonic approximation.

The shape of the absorption/emission spectrum at low temperatures is easily obtained within the adiabatic and Condon approximations. The electron-phonon interaction is considered as a perturbation in the electron equation of the adiabatic approximation, and zero order electronic functions are exploited in calculations. The absorption coefficient $K_{ab}(\Omega)$ at the radiation frequency Ω for the electric dipole $a(4f^n)\rightarrow b(4f^{n-1}5d)$ transition, allowed in the Condon approximation, is proportional to the product of the normalized absorption form function[38]

$$F_{ab}(\Omega)=2\pi e^{-S_b}\sum_{p=0}^{\infty} M_{p,b}(\Omega-\Omega_{ba}) \tag{6}$$

and the integral intensity of the transition given by $|\langle b(5d)|\mathbf{d}\boldsymbol{\varepsilon}|a(4f)\rangle|^2$, where $\boldsymbol{\varepsilon}$ is the polarization vector of radiation, $\boldsymbol{d}$ is the effective electric dipole moment of an ion, $M_{p,b}$ represents a p-phonon contribution to the spectrum: $M_{0,b}(\Omega-\Omega_{ba})=\delta(\Omega-\Omega_{ba})$, and for $p>0$ and any b_1, b_2, b_3, b_4 states from the $4f^{n-1}5d$ configuration

$$M_{p,b}(\Omega-\Omega_{ba}) = \frac{1}{(\pi\hbar)^p p!}\int \frac{d\omega_1}{\omega_1^2}\cdots\frac{d\omega_p}{\omega_p^2} D_{bbbb}(\omega_1)\ldots D_{bbbb}(\omega_p) \times\delta(\Omega-\Omega_{ba}-\omega_1\ldots-\omega_p), \tag{7}$$

$$D_{b_1b_2b_3b_4}(\omega) = \sum_{Ls\alpha} \sum_{L's'\beta} \langle b_1|V_\alpha(Ls)|b_2\rangle g_{\alpha\beta}(Ls,L's'|\omega) \times \langle b_3|V_\beta(L's')|b_4\rangle^* . \quad (8)$$

The form function of the emission spectrum is obtained from (6) by substituting $2\Omega_{ba}-\Omega$ for Ω. Functions $g_{\alpha\beta}(Ls,L's'|\omega)$ in Eq. (8) represent spectral densities of correlation functions for the relative dynamic displacements of ions in the cluster.[35] The integral intensity of a ZPL at the frequency Ω_{ba}, which corresponds to the energy gap E_b-E_a (E is the crystal field energy) diminished by the Jahn-Teller (JT) energy $E_{JT}(b)=-\frac{1}{\pi}\int D_{bbbb}(\omega)\frac{d\omega}{\omega}$, is determined by the Huang-Rhys parameter $S_b=\frac{1}{\pi\hbar}\int D_{bbbb}(\omega)\frac{d\omega}{\omega^2}$. The effective number of p-phonon bands, to be considered explicitly in the simulation of the form-function $F_{ab}(\Omega)$, may be approximated as $p_{\max}=2S_b$.

To derive the absorption/emission form-function at the radiation frequency Ω for the spin-forbidden electric dipole $a(4f^n)\leftrightarrow b(4f^{n-1}5d)$ transitions, we consider the electronic wave function of the b state in the first order in perturbation $H_{el\text{-}ph}$. The corresponding non-Condon form function is determined by dynamic admixture of all other $4f^{n-1}5d$ states to the b state, and can be obtained in the following form:

$$K_{ab}^{(f)}(\Omega) \sim F_{ab}(\Omega)\left|\int \varphi(\omega)d\omega\right|^2 + \int F_{ab}(\Omega \mp \omega) \times \left\{f(\omega) \mp 2\mathrm{Re}\left[\varphi(\omega)\int \varphi(\omega')^* d\omega'\right]\right\}d\omega + \int\int F_{ab}(\Omega \mp \omega \mp \omega')\varphi(\omega)\varphi(\omega')^* d\omega d\omega', \quad (9)$$

where upper and lower signs should be used for the absorption and emission, respectively, and

$$f(\omega) = \sum_{c',c\neq b} \frac{\langle c|\mathbf{d}\boldsymbol{\varepsilon}|a\rangle\langle c'|\mathbf{d}\boldsymbol{\varepsilon}|a\rangle^*}{(E_b-E_c)(E_b-E_{c'})}\frac{\hbar}{\pi}D_{cbc'b}(\omega), \quad (10)$$

$$\varphi(\omega) = \sum_{c\neq b} \frac{\langle a|\mathbf{d}\boldsymbol{\varepsilon}|c\rangle}{E_b-E_c}\frac{1}{\pi\omega}D_{cbbb}(\omega). \quad (11)$$

Here the sums are taken over all $4f^{n-1}5d$ states, different from the state b. Unlike the case of the allowed transitions, not only the integral intensities of the forbidden $a(4f^n)\leftrightarrow b(4f^{n-1}5d)$ spectral bands depend on the a state, but also their line shapes, even though we neglect the electron-phonon interaction in the $a(4f^n)$ state. As it follows from Eq. (9), a possibility to observe directly the form function $F_{ab}(\Omega)$ and the corresponding ZPL at the frequency Ω_{ba} depends on the dimensionless ratios $|\int D_{cbbb}(\omega)\frac{d\omega}{\pi\omega}/(E_c-E_b)|$ which may be essentially less than unity due to lower values of spectral cross-distributions $D_{cbbb}(\omega)$ in comparison with the autodistributions $D_{bbbb}(\omega)$ and $D_{cbcb}(\omega)$. In a general case, the mirror symmetry between the spin-forbidden absorption and emission spectra is broken due to different signs of the third term at the rhs of Eq. (9).[38]

TABLE I. Spin-orbit coupling constants and crystal field parameters in $LiYF_4:Ce^{3+}$ and $LiYF_4:Lu^{3+}$ (in cm^{-1}).

	Ce^{3+}	Lu^{3+}
$\zeta(4f)$	625	3406
$B_0^2(4f)$	360	380
$B_0^4(4f)$	−1400	−600
$B_4^4(4f)$	−1240+750i	−590+510i
$B_0^6(4f)$	−67.2	−36.8
$B_4^6(4f)$	−1095+458i	−413+254i
$\zeta(5d)$	1082	1939
$B_0^2(5d)$	2454	2207
$B_0^4(5d)$	−16494	−13027
$B_4^4(5d)$	−17323+17020i	−13515+13332i

2. *Simulations of the electron-vibrational spectra in* $LiYF_4:Ce^{3+}$ *and* $LiYF_4:Lu^{3+}$

Following the general approach described above, we have calculated the energy level patterns of the excited configurations and shapes of the electron-vibrational f-d absorption and emission spectra at low temperatures for the impurity Ce^{3+} and Lu^{3+} ions in $LiYF_4$.

Trivalent RE ions substitute for Y^{3+} ions in $LiYF_4$ crystals in sites with S_4 point symmetry. The energy level patterns of the excited configurations $5d^1$ (Ce^{3+}) and $4f^{13}5d^1$ (Lu^{3+}) contain five Kramers doublets (in the tetragonal crystal field, the $5d$ orbital manifold splits into three singlets and a doublet which is split further by the spin-orbit interaction), and 70 singlets and 35 non-Kramers doublets, respectively.

Parameters used in the calculations of the crystal field energies of the excited Ce^{3+} and Lu^{3+} configurations are listed in Table I. The spin-orbit coupling constants $\zeta(4f)$ and $\zeta(5d)$ were taken from the literature.[39,40] The crystal field parameters were calculated using the analytical radial $5d$ functions from Refs. 41 and 42 and $2s$, $2p$ functions of the F^- ion from Ref. 43. Ion charges were fixed as −1 (F^-), +1 (Li^+), +3 (Y^{3+}). Parameters of the exchange charge model $G_s=1.69$ (Ce^{3+}) and 1.55 (Lu^{3+}), $G_\sigma=2.45$ and $G_\pi=0.13$, the overall energy shift of the $5d$ configuration $\Delta=43\,827$ and $104\,493$ cm^{-1} for Ce^{3+} and Lu^{3+}, respectively, and the parameters of the Coulomb [$F^{(2)}(fd)=19\,727$ cm^{-1}, $F^{(4)}(fd)=10\,477$ cm^{-1}] and exchange [$G^{(1)}(f\,d)=4662$ cm^{-1}, $G^{(3)}(f\,d)=5640$ cm^{-1}, $G^{(5)}(f\,d)=7087$ cm^{-1}] interactions between the electrons (for the Lu^{3+} ion) were obtained from fitting the calculated spectra to the experimental data. Since the shift of a vibronic band maximum from a ZPL roughly compensates for the Jahn-Teller energy, the calculated crystal field energies were fitted to the positions of the corresponding vibronic band maxima. For the impurity Ce^{3+} centers, a radial local deformation of the crystal lattice was taken into account (the RE ion – ligand distances were enlarged by about 3%).[44]

TABLE II. Spectral characteristics of the low-energy Lu^{3+} $4f^{13}5d$ states.

State Number	E_{CF} (cm^{-1})	E_{JT} (cm^{-1})	E (ZPL) (cm^{-1})	The Huang-Rhys parameter	Relative intensity $\sigma(\varepsilon \| a)$	Relative intensity $\pi(\varepsilon \| c)$
1	81391	−263	81127	1.29	0 ($1.54\cdot10^{-3}$)	0 ($6\cdot10^{-4}$)
2	81404	−264	81140	1.29	0 ($1.76\cdot10^{-3}$)	0 ($6\cdot10^{-3}$)
3, 4	82154	−205	81950	0.96	0.530	0
5	82620	−162	82458	0.73	0	$5\cdot10^{-5}$
6, 7	83649	−300	83349	1.49	6.444	0
8	83923	−326	83597	1.63	0	2.057
9	84218	−269	83950	1.31	0	0.003
10, 11	84339	−288	84052	1.41	0.181	0
12	84541	−257	84285	1.23	0	3.872
14, 15	84903	−235	84667	1.12	0.923	0

The correlation functions for relative displacements of the impurity RE^{3+} ion and its nearest neighbors were computed in the framework of the lattice dynamics model of the $LiYF_4$ crystal derived in Ref. 27. To compare the simulated spectral envelopes with the measured spectra, form-functions (7) were convoluted with a Gaussian to take into account the inhomogeneous broadening (~25 cm^{-1}) induced by random lattice strains and with a Lorentz distribution to account for the relaxation broadening (the homogeneous widths were estimated from calculations of spontaneous one-phonon transition probabilities).

The calculated integral intensities and positions of the maxima of the electron-vibrational $4f$-$5d$ bands in the ground state absorption spectra of $LiYF_4:Ce^{3+}$ at low temperatures agree satisfactorily with the experimental data.[35,45] The calculated Huang-Rhys parameters for the $5d$ crystal field states of Ce^{3+} ion in $LiYF_4$ equal 2.9, 17.4, 6.0, 6.0, 16.4, with the smallest value for the lowest $5d$ state, thus explaining why the ZPL is observed only in the transitions which involve this state, while all other $4f$-$5d$ bands can be approximated well by smooth Gauss distributions with different widths.[45] The simulated line shape for the $4f$-$5d$ absorption to the lowest $5d$ state in $LiYF_4:Ce^{3+}$ with the well pronounced fine structure is in a good agreement with the measured shape of the excitation spectrum of Ce^{3+} luminescence in $LiGdF_4:Ce^{3+}$ (Fig. 7) as well.

The calculated crystal field energies of the Lu^{3+} $4f^{13}5d$ configuration spread over the range 81 000 cm^{-1} – 113 000 cm^{-1}, with nearly 90% of absorption intensity being in the second half of the spectrum. The structure of the spectrum follows general regularities found in the spectra of RE-doped $LiYF_4$ crystals.[35] Three groups of states can be distinguished: 16 states from 81 000 to 84 700 cm^{-1}, weakly coupled to phonons (with the Huang-Rhys parameters from 0.7 to 1.6); 16 states from 87 400 to 90 700 cm^{-1}, strongly coupled to phonons (with the Huang-Rhys parameters from 4.5 to 7.6); the continuum of mixed electron-phonon states distributed in the range of energies from 93 000 to 113 000 cm^{-1}, with the Huang-Rhys parameters varying from 0.4 to 7 (these levels interact strongly with the nonadiabatic phonons).

The observed excitation spectrum (see Fig. 8) corresponds to the first group of the $4f^{13}5d$ states. In Table II we present calculated characteristics for the states from this group, which have nonzero absorption intensity: the number of a state, the crystal field energy E_{CF}, the Jahn-Teller energy E_{JT}, the ZPL frequency, the Huang-Rhys parameter, and the relative integral intensities of the σ and π polarized electric-dipole transitions [the squared matrix elements of the first rank spherical operators between the $^1S_0(4f^{14})$ ground state and the corresponding $4f^{13}5d$ state].

The simulated (the inhomogeneous broadening width of 28 cm^{-1} was introduced) nonpolarized absorption spectrum corresponding to allowed transitions from $^1S_0(4f^{14})$ to lower sublevels of the $4f^{13}5d$ configuration of Lu^{3+} in $LiYF_4$ is compared with the experimental excitation spectrum in Fig.

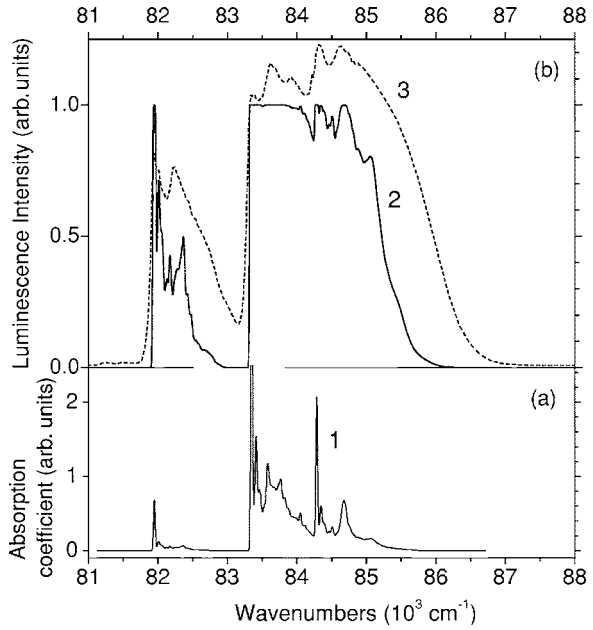

FIG. 11. (a) The low temperature simulated Lu^{3+} $4f$-$5d$ spin-allowed absorption spectrum (1, thin solid curve). (b) The modeled (2, bold solid curve) and the measured (3, dashed curve) excitation spectra of $LiYF_4:Lu^{3+}$(5%).

11. At first sight, there seems to be a significant discrepancy in calculated and experimental transition intensities. However, we have to take into consideration that $LiYF_4:Lu^{3+}(5\%)$ reaches optical saturation at least in the peaks of the spin- and parity-allowed $4f$-$5d$ transitions. Therefore, from the theoretical absorption curve $K(\Omega)$, the actual excitation spectrum has been estimated by $\{1-\exp[-K(\Omega)d]\}$, where d is the crystal thickness (curve 2 in Fig. 11). As the absorption curve was calculated in arbitrary units, d was treated as a parameter. It was adjusted in a way that the relative height of the main maxima is reproduced. The overall agreement is satisfactory, though it is clear that the simulated ZPLs are more pronounced than the measured ones; the reason for the discrepancy may be that we have not taken into account interactions of crystal field doublets with nonadiabatic phonons.

The low energy intensive band in the excitation spectrum of $LiYF_4:Lu^{3+}(5\%)$, with a narrow line at 81 950 cm^{-1}, is ascribed to the spin-allowed transitions to the lowest (3,4) doublet. The energy gap Δ was chosen so that the corresponding ZPL coincides with the observed narrow line. The maximum of the simulated vibronic band is at 82 327 cm^{-1}, greater than the experimental value by about 100 cm^{-1}. The next intensive band in the excitation spectrum has 5 pronounced maxima. We list their energies with the assignment (the state number) in parentheses: 83 345 cm^{-1} (6,7 – ZPL), 83 620 cm^{-1} (8 – ZPL, 6,7 - vibronic band), 83 920 cm^{-1} (9 – ZPL; the maximum is not reproduced well due to the underestimated transition intensity), 84 320 cm^{-1} (12 – ZPL), 84 620 cm^{-1} (14,15 – ZPL, 12 – vibronic band).

The intensities of transitions from the ground state $^1S_0(4f^{14})$ to the lowest quasidoublet (1,2) in the $4f^{13}5d$ configuration equal zero (in Condon approximation), however the corresponding ZPL energies are at the threshold of the weak feature in the observed excitation spectrum (see Fig. 8). Besides, the first state is positioned in the middle between the first feature in the emission spectrum (81 035 cm^{-1}) and the first maximum of the weak feature in the excitation spectrum (81 240 cm^{-1}). This supports the hypothesis of Sec. III B 2, that the phonon-assisted spin-forbidden $4f^{14}$-$4f^{13}5d$ transitions are observed in these spectra.

We simulated the absorption and emission spectra for the forbidden transitions utilizing Eqs. (9)–(11). The results of calculations are compared with the weak feature observed in $LiYF_4:Lu^{3+}(5\%)$ excitation spectrum and with the $LiYF_4:Lu^{3+}(0.5\%)$ emission spectrum in Fig. 12. The agreement is satisfactory, especially for the emission spectrum (no additional fitting has been done). Only the term $\int F_{ab}(\Omega-\omega)f(\omega)d\omega$ brings about significant contribution to the form function $K_{ab}^{(f)}(\Omega)$ [see Eq. (9)] for the forbidden transitions under investigation. This explains the absence of the ZPLs in experimental emission and excitation spectra corresponding to the spin-forbidden transitions in $LiYF_4:Lu^{3+}$, and leads to symmetric calculated spin-forbidden absorption and emission spectra. The fine structure in the calculated spectra comes from a convolution of the ZPL in $F_{ab}(\Omega)$ with $f(\omega)$ and reproduces the spectral distributions of the electron-phonon coupling between the lowest quasidoublet and other crystal field states in the excited configuration. Other terms in $F_{ab}(\Omega)$ lead to higher order convolutions of $g_{\alpha\beta}(Ls,L's'|\omega)$ spectral densities, with the fine structure smoothed out.

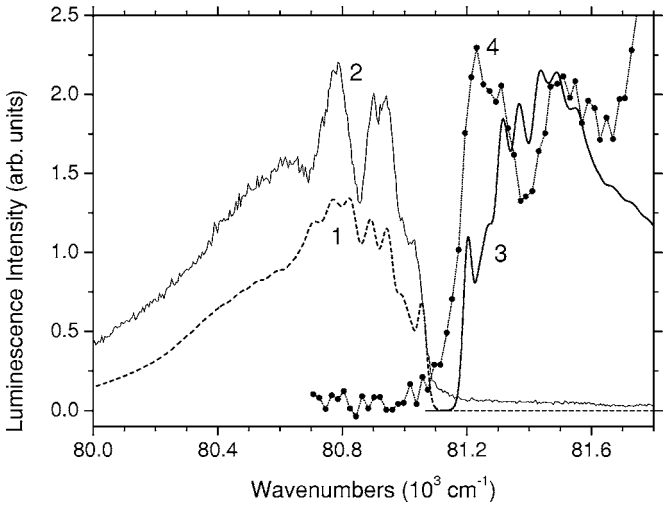

FIG. 12. The low temperature simulated (1, dashed curve) and measured (2, thin solid curve) emission spectra; simulated (3, bold solid curve) and measured (4, dotted curve) excitation spectra in the region of Lu^{3+} $4f$-$5d$ spin-forbidden transitions in $LiYF_4:Lu^{3+}$.

The calculated integral intensities of phonon-induced electric dipole transitions involving the first and the second $4f^{13}5d$ states, defined by $\int f(\omega)d\omega$, are given in parentheses in Table II. The magnitude of the simulated nonpolarized excitation curve for the forbidden transitions is of the same order as the experimental one, once the scaling coefficient was established in Fig. 11.

IV. CONCLUSIONS

The VUV $4f^{n-1}5d$-$4f^n$ luminescence and luminescence excitation spectra of various Gd^{3+} and Lu^{3+} containing fluorides have been analyzed with high spectral resolution. Gd^{3+} ions emit only fast (nanosecond) spin-allowed $5d$-$4f$ luminescence as it is typical for RE^{3+} ions from the first half of the lanthanide series. At low temperatures, Lu^{3+} ions emit exclusively slow spin-forbidden $5d$-$4f$ luminescence. With increasing temperature, however, an admixture of spin-allowed $5d$-$4f$ emission shows up. Strong electron-phonon coupling has been observed from REF_3-type systems, whereas the spectra of the more complex $LiREF_4$ systems exhibit intermediate coupling with zero-phonon lines (Gd^{3+}) and phonon sidebands.

Spectral envelopes of some of the spectra have been simulated as well. Contrary to earlier attempts to calculate VUV $5d$-$4f$ luminescence and luminescence excitation spectra where electron-phonon interaction was simulated with Gaussian broadening of electronic excitations and Gaussian sidebands in luminescence,[45] the present theoretical results originate from a microscopic semiphenomenological model of the crystal field and the crystal lattice vibrational spectrum. The simulations were restricted to the Ce^{3+} and Lu^{3+} ions with simple $4f^0 5d$ and $4f^{13}5d$ electronic configura-

tions, respectively. Good agreement between experiment and theory was achieved. The absence of a ZPL in the Lu^{3+} spectra with intermediate electron-phonon coupling was also obtained from the simulation of the spin-forbidden spectrum. Concerning the more complicated case of Gd^{3+} with its $4f^6 5d$ electronic configuration, the luminescence spectra were calculated in an indirect way. Based on the observation that the Gd^{3+} $5d$-$4f$ luminescence spectrum in $LiYF_4$ is very similar to the excitation spectrum of the Ce^{3+} $5d$-$4f$ emission in the same host, the spectra were calculated for the Ce^{3+} ion. In this way, it was possible to identify the phonon structures in the Gd^{3+} luminescence spectra. It is the *combination* of the high-resolution spectra with their theoretical treatment that brought about an understanding of Gd^{3+} and Lu^{3+} $5d$-$4f$ luminescence and luminescence excitation in various fluoride-type hosts.

ACKNOWLEDGMENTS

The authors would like to thank J. Y. Gesland and J. C. Krupa for supplying us with some of the investigated samples. The support by RFBR Grant No. 05-02-17306, by the Estonian Science Foundation (Grant No. 6538), by the Ministry of Education and Science of the Russian Federation (project RNP 2.1.1.7348), and by the European Community Research Infrastructure Action within the FP6 Program, Contract No. RII3-CT-2004-506008 (IA-SFS) is gratefully acknowledged.

*Electronic address: makhov@sci.lebedev.ru

[1] P. P. Feofilov, Opt. Spectrosc. **1**, 992 (1956).
[2] A. A. Kaplyanskii and P. P. Feofilov, Opt. Spectrosc. **13**, 129 (1962).
[3] A. A. Kaplyanskii, V. N. Medvedev, and P. P. Feofilov, Opt. Spectrosc. **14**, 664 (1963).
[4] E. Loh, Phys. Rev. **147**, 332 (1966).
[5] W. M. Yen, L. R. Elias, and D. L. Huber, Phys. Rev. Lett. **24**, 1011 (1970).
[6] G. Zimmerer, J. Lumin. **119-120**, 1 (2006).
[7] L. R. Elias, W. S. Heaps, and W. M. Yen, Phys. Rev. B **8**, 4989 (1973).
[8] W. S. Heaps, L. R. Elias, and W. M. Yen, Phys. Rev. B **13**, 94 (1976).
[9] K. H. Yang and J. A. DeLuca, Appl. Phys. Lett. **29**, 499 (1976).
[10] R. T. Wegh, H. Donker, and A. Meijerink, Phys. Rev. B **57**, R2025 (1998).
[11] R. T. Wegh and A. Meijerink, Phys. Rev. B **60**, 10820 (1999).
[12] M. Kirm, J. C. Krupa, V. N. Makhov, M. True, S. Vielhauer, and G. Zimmerer, Phys. Rev. B **70**, 241101(R) (2004).
[13] M. Kirm, V. N. Makhov, M. True, S. Vielhauer, and G. Zimmerer, Phys. Solid State **47**, 1416 (2005).
[14] V. N. Makhov, J. C. Krupa, M. Kirm, G. Stryganyuk, S. Vielhauer, and G. Zimmerer, Russ. Phys. J. **4**(suppl.), 85 (2006).
[15] G. H. Dieke and H. M. Crosswhite, Appl. Opt. **2**, 675 (1963).
[16] G. Zimmerer, Nucl. Instrum. Methods Phys. Res. A **308**, 178 (1991).
[17] Y. Chen, M. Kirm, E. Negodin, M. True, S. Vielhauer, and G. Zimmerer, Phys. Status Solidi B **240**, R1 (2003).
[18] M. Louis, E. Simoni, S. Hubert, and J. Y. Gesland, Opt. Mater. **4**, 657 (1995).
[19] R. Yu. Abdulsabirov, A. A. Kazantsev, S. L. Korableva, B. Z. Malkin, S. I. Nikitin, and A. L. Stolov, J. Lumin. **117**, 225 (2006).
[20] R. T. Wegh, H. Donker, A. Meijerink, R. J. Lamminmäki, and J. Hölsä, Phys. Rev. B **56**, 13841 (1997).
[21] H. M. Crosswhite, R. L. Schwiesow, and W. T. Carnall, J. Chem. Phys. **50**, 5032 (1969).
[22] C. Görller-Walrand, K. Binnemans, and L. Fluyt, J. Phys.: Condens. Matter **5**, 8359 (1993).
[23] P. Dorenbos, J. Lumin. **91**, 91,155 (2000).
[24] N. Yu. Kirikova, M. Kirm, J. C. Krupa, V. N. Makhov, E. Negodine, and J. Y. Gesland, J. Lumin. **110**, 135 (2004).
[25] P. S. Peijzel, A. Meijerink, R. T. Wegh, M. F. Reid, and G. W. Burdick, J. Solid State Chem. **178**, 448 (2005).
[26] W. T. Carnall, P. R. Fields, and R. Sarup, J. Chem. Phys. **57**, 43 (1972).
[27] S. Salaün, M. T. Fornoni, A. Bulou, M. Rousseau, P. Simon, and J. Y. Gesland, J. Phys.: Condens. Matter **9**, 6941 (1997).
[28] M. M. Lage, A. Righi, F. M. Matinaga, J. Y. Gesland, and R. L. Moreira, J. Phys.: Condens. Matter **16**, 3207 (2004).
[29] A. N. Vasil'ev and V. V. Mikhailin, *Introduction in Solid State Spectroscopy* (Moscow University Press, Moscow, 1987).
[30] V. N. Makhov, M. Kirm, and G. Stryganyuk, Radiation Measurements (to be published).
[31] F. M. Ryan, W. Lehmann, D. W. Feldman, and J. Murphy, J. Electrochem. Soc. **121**, 1475 (1974).
[32] A. Ellens, A. Meijerink, and G. Blasse, J. Lumin. **59**, 293 (1994).
[33] L. van Pieterson, M. F. Reid, G. W. Burdick, and A. Meijerink, Phys. Rev. B **65**, 045114 (2002).
[34] V. N. Makhov, N. M. Khaidukov, N. Yu. Kirikova, M. Kirm, J. C. Krupa, T. V. Ouvarova, and G. Zimmerer, J. Lumin. **87-89**, 1005 (2000).
[35] B. Z. Malkin, O. V. Solovyev, A. Yu. Malishev, and S. K. Saikin, J. Lumin (to be published).
[36] B. Z. Malkin, in *Spectroscopy of solids containing rare-earth ions*, edited by A. A. Kaplyanskii and R. M. Macfarlane (Elsevier Science Publishers, Amsterdam, 1987), Ch. 2, p. 13.
[37] D. Garcia and M. Faucher, Phys. Rev. B **30**, 1703 (1984).
[38] Yu. E. Perlin and B. S. Tzukerblat, *Electron-vibrational interaction effects on optical spectra of impurity paramagnetic ions* (Kishinev, Stiintza, 1974).
[39] M. F. Reid, L. van Pieterson, and A. Meijerink, J. Alloys Compd. **344**, 240 (2002).
[40] J. Sugar and V. Kaufman, J. Opt. Soc. Am. **62**, 562 (1972).
[41] N. V. Starostin, in *Spectroscopy of crystals* (Nauka, Moskva, 1975), p. 12.
[42] N. V. Starostin, P. F. Gruzdev, E. P. Pashnina, and V. A. Ganin, in *Spectroscopy of crystals* (Nauka, Moskva, 1975), p. 216.
[43] E. Clementi and A. D. McLean, Phys. Rev. **133**, A419 (1964).
[44] M. Stephan, M. Zachau, M. Groting, O. Karplak, V. Eyert, K. C. Mishra, and P. C. Schmidt, J. Lumin. **114**, 255 (2005).
[45] M. F. Reid, L. van Pieterson, R. T. Wegh, and A. Meijerink, Phys. Rev. B **62**, 14744 (2000).